A fungal powdery mildew pathogen induces extensive local and marginal systemic changes in the *Arabidopsis thaliana* microbiota

Paloma Durán [1,2], Anja Reinstädler [3], Anna Lisa Rajakrut [1], Masayoshi Hashimoto [4], Ruben Garrido-Oter [1,2,5], Paul Schulze-Lefert [1,2,5], Ralph Panstruga [3,5]

[1] Max Planck Institute for Plant Breeding Research, Department of Plant-Microbe Interactions, Carl-von-Linné-Weg 55, 50829 Cologne, Germany

[2] Cluster of Excellence on Plant Sciences, 40225 Düsseldorf, Germany.

[3] RWTH Aachen University, Institute for Biology I, Unit of Plant Molecular Cell Biology, Worringerweg 1, 52056 Aachen, Germany

[4] Graduate School of Agricultural and Life Sciences, The University of Tokyo, 113-8657 Tokyo, Japan.

[5] co-corresponding authors

Summary

• Powdery mildew is a foliar disease caused by epiphytically growing obligate biotrophic ascomycete fungi. How powdery mildew colonization affects host resident microbial communities locally and systemically remains poorly explored.

• We performed powdery mildew (*Golovinomyces orontii*) infection experiments with *Arabidopsis thaliana* grown in either natural soil or a gnotobiotic system and studied the influence of pathogen invasion into standing natural multi-kingdom or synthetic bacterial communities (SynComs).

• We found that after infection of soil-grown plants, *G. orontii* outcompetes numerous resident leaf-associated fungi. We further detected a significant shift in foliar but not root-associated bacterial communities in this setup. Pre-colonization of germ-free *A. thaliana* leaves with a bacterial leaf-SynCom, followed by *G. orontii* invasion, induced an overall similar shift in the foliar bacterial microbiota and minor changes in the root-associated bacterial assemblage. However, a standing root SynCom in root samples remained robust against foliar infection with *G. orontii*. Although pathogen growth was unaffected by the leaf SynCom, fungal infection caused a more than two-fold increase in leaf bacterial load.

• Our findings indicate that *G. orontii* infection affects mainly microbial communities in local plant tissue, possibly driven by pathogen-induced changes in source-sink relationships and host immune status.

Keywords:

Arabidopsis thaliana, *Golovinomyces orontii*, gnotobiotic plant system, microbial multi-kingdom interactions, plant microbiota, powdery mildew, synthetic community

39 **Abbreviations**

40 ASV	Amplificon sequence variant
41 ITS	Internal transcribed spacer
42 PCoA	Principal coordinates analysis
43 RA	Relative abundance
44 SynCom	Synthetic community

45

46

Introduction

Unlike plants grown under germ-free laboratory conditions, healthy plants in nature live in association and interact with a multitude of microorganisms belonging to several microbial classes, such as bacteria, fungi, oomycetes and protists, collectively called the plant microbiota (Bulgarelli *et al.*, 2013). Marker gene amplicon sequencing has served as an important tool for taxonomic profiling and quantitative surveys of microbial assemblages associated with different plant organs over a range of environmental and experimental conditions, revealing community composition and major factors explaining community structure (Hacquard & Schadt, 2015; Thiergart *et al.*, 2020). Root-associated bacterial assemblages, assessed by amplicon sequencing of the *16S* rRNA marker gene, are defined by a specific subset of bacteria that originate mainly from the highly diverse soil biota. These communities are characterized by a robust taxonomic pattern at the phylum rank, which comprises the dominant Proteobacteria as well as Actinobacteria, Bacteroidetes, and Firmicutes (Bulgarelli *et al.*, 2012; Lundberg *et al.*, 2012; Hacquard & Schadt, 2015). The main factors governing differences in root assemblages are, in order of importance, soil type (edaphic factors such as pH), plant species/genotype, and plant age (Lauber *et al.*, 2009; Hacquard *et al.*, 2015; Müller *et al.*, 2016; Finkel *et al.*, 2017). For leaf-associated bacterial assemblages, the seeding source is less defined because microbiota members can originate from aerosols, insects, and soil as well as upward microbial migration from the root (Vorholt, 2012; Müller *et al.*, 2016). Although root- and leaf-associated microbiota share a similar phylum-level taxonomic composition, the overall community structure in leaves is subject to larger fluctuations. Similar to bacterial communities, plant-associated fungi have been studied at the community level by amplicon sequencing of the internal transcribed spacer (ITS) region between the small- and large-subunit rRNA genes or the *18S* rRNA gene (Bazzicalupo *et al.*, 2013). Plant-associated fungal assemblages are dominated by members belonging to the Ascomycota and Basidiomycota phyla, and these communities display more stochastic variation compared with the bacterial microbiota, with biogeography as the strongest explanatory factor (Coleman-Derr *et al.*, 2016; Gao *et al.*, 2020; Thiergart *et al.*, 2020). In fact, taxonomically structured microbial communities with similar taxa on each plant individual have been described until now only for the bacterial root microbiota (Lundberg *et al.*, 2012).

Systematic establishment of plant-derived microbial culture collections of the plant microbiota has enabled microbiota reconstitution experiments with germ-free plants and taxonomically representative synthetic communities (SynComs) that can be used to address principles underlying community assembly and proposed microbiota functions under defined laboratory environments. This experimental approach has proven critical to the advancement of microbiota research (Bai *et al.*, 2015; Lebeis *et al.*, 2015; Durán *et al.*, 2018; Zhang *et al.*, 2019a). For example, more than 400 leaf- and root-derived bacterial commensals have been isolated from healthy *A. thaliana* grown in natural soil, comprising 35 bacterial families belonging to the aforementioned four phyla (Bai *et al.*, 2015). This microbiota culture collection represents the majority of bacterial taxa that are detectable by culture-independent *16S* rRNA gene community profiling in the *A. thaliana* phyllo- and rhizosphere. Microbiota reconstitution experiments using SynComs from this collection revealed that the bacterial root microbiota provides indirect protection to its host against soil-borne and root-associated harmful fungi and that this protection is essential for plant survival (Duran et al., 2018). Similar reconstitution experiments have shown that bacterial root commensals are necessary for iron nutrition of *A. thaliana* in naturally occurring calcareous soils, where poor bioavailability of this soil mineral nutrient limits plant growth (Harbort *et al.*, 2020).

Relatively little is known about how the plant microbiota responds to pathogen invasion. The oomycete leaf pathogen *Albugo* has strong effects on epiphytic and endophytic bacterial colonization in *A. thaliana*. Specifically, α-diversity decreased and β-diversity stabilized in the presence of *Albugo* infection in leaves, whereas they otherwise varied between plants (Agler *et al.*, 2016). The effect of *Alb. laibachii* on leaf-associated fungal communities were less consistent and not as clear. Upon foliar defense activation by the downy mildew oomycete pathogen *Hyaloperonospora arabidopsidis*, the host *A. thaliana* specifically promotes three bacterial species in the rhizosphere, namely *Xanthomonas*, *Microbacterium*, and *Stenotrophomonas* sp., respectively (Berendsen *et al.*, 2018). Although separately these bacteria did not affect the host significantly, together they induced systemic resistance against downy mildew and promoted growth of the plant.

The analysis of powdery mildew-induced changes in plant leaf microbiota so far rests on field studies with powdery mildew-infected leaf samples (diseased leaves) in comparison to healthy/less infected leaves in Japanese spindle (*Euonymous japonicus*) (Zhang *et al.*, 2019b),

110 pumpkin (*Cucurbita moschata*) (Zhang *et al.*, 2018) and English oak (*Quercus robur*)
111 (Jakuschkin *et al.*, 2016) (reviewed in (Panstruga & Kuhn, 2019)). In the *E. japonicus* study,
112 the authors noticed a reduction in bacterial and fungal diversity, associated with a general
113 decrease in relative abundance (RA) at the genus level (Zhang *et al.*, 2019b). Similarly, the
114 richness and diversity of the fungal community was found to be reduced in pumpkin leaves
115 heavily infected by powdery mildew (*Podospharea* sp.) (Zhang *et al.*, 2018). Marked changes
116 in the composition of foliar fungal and bacterial communities were also observed in *Erysiphe*
117 *alphitoides*-colonized oak (Jakuschkin *et al.*, 2016). However, all these studies rely on field
118 samples and natural powdery mildew infections in fluctuating conditions, which complicates
119 deconvolution of microbiota changes caused by changes in environmental factors from
120 those driven by pathogen infection.

121 Here, we examined the effect of controlled powdery mildew (*G. orontii*) infection on the
122 structure of *A. thaliana* leaf and root microbiota in either soil-grown plants or a gnotobiotic
123 plant system pre-treated with defined root- or leaf SynComs. In both settings, we found
124 major powdery mildew-induced shifts in the composition of the local (foliar) assemblages of
125 fungal (natural soil) and bacterial (natural soil and sterile conditions) communities. In the
126 case of the leaf SynCom, this shift was also associated with a marked increase in bacterial
127 load. Apart from these major changes in the phyllosphere, we also observed a minor
128 systemic effect on the structure of the bacterial root microbiota in conjunction with the leaf
129 SynCom and powdery mildew challenge.

130

131 **Materials and Methods**

132 **Plant material**

133 *A. thaliana* Col-0 wild-type (Arabidopsis stock centre accession N60000) was used as model
134 plant system. Seeds were surface-sterilized by treating them with 70% for 20 min and drying
135 them under a sterile hood. Subsequently, the seeds were stratified overnight at 4 °C.

136 **Microbial strains**

137 The *At*-SPHERE bacterial strains used in this study have been previously reported (Bai *et al.*,
138 2015) and are summarized in Table S1. *G. orontii* (isolate MPIPZ) was used as powdery mildew
139 infection agent. *G. orontii* was regularly propagated every week on 4- to 5-week-old
140 supersuceptible *A. thaliana eds1* plants. Powdery mildew inoculation was conducted by leaf-
141 to-leaf contact of healthy plants with rosette leaves of heavily infected *eds1* plants as reported
142 previously (Acevedo-Garcia *et al.*, 2017).

143 **Natural soil experiment**

144 *A.thaliana* Col-0 seeds were sown into 7x7 greenhouse pots filled with Cologne Agricultural
145 Soil (CAS) batch 12 and grown under short-day greenhouse conditions for 6.5 weeks (12 pots
146 containing 5 seeds each). Then, half of the plants were inoculated with *G. orontii* and all pots
147 were transferred to a growth chamber (day: 21 °C, 10 h light; night: 19 °C; 70% humidity). At
148 11 days post inoculation (dpi), bulk soil, rhizosphere, root and leaf samples were harvested as
149 previously described (Figure 1A; (Bulgarelli *et al.*, 2012; Bai *et al.*, 2015)).

150 **SynCom experiments in gnotobiotic system**

151 Calcined clay was washed several times with tap water followed by MiliQ water. After
152 removal of the liquid, the calcined clay was autoclaved following a liquid cycle (121 °C, 20
153 min), and oven-dried at 60 °C for 4 weeks. Of the washed, autoclaved and dried calcined clay,
154 100 g were transferred into a previously sterilized Magenta GA-7 plant culture box (Thermo
155 Fisher Scientific, Schwerte, Germany), sealed and autoclaved again, and dried overnight prior
156 to the experiment.

157 The bacterial strains used were pre-grown for 7 d in Tryptic Soy Broth 50 % (TSB 50 %, Sigma-
158 Aldrich), and washed with 10 mM $MgCl_2$ (series of centrifugations and removal of
159 supernatant, and final resuspension in $MgCl_2$) to remove any byproducts from the bacterial

160 cultures. A total of 88 and 103 bacterial strains were selected, which were differentiable
161 based on the their *16S* sequence (see Table S1), for the root and leaf SynComs, respectively,
162 and mixed in three separate inputs. For each of the three bacterial mixes, the OD_{600} was set
163 to 0.5 (root SynCom) and to 0.2 (leaf SynCom) with 10 mM $MgCl_2$. A sample of each of the
164 bacterial inputs was taken as a reference for bacterial community composition.

165 For the root SynCom, 70 mL ½ MS media (including vitamins without sucrose, pH 7, Sigma-
166 Aldrich GmbH, CatNo M5524-1L, Taufkirchen, Germany) were mixed with 1 mL of the SynCom
167 culture and used to inoculate one calcined-clay-containing Magenta box (n=12). As a control,
168 to a separate batch of magenta boxes only ½ MS media without SynCom culture was added
169 (n=12). Surface- sterilized *A. thaliana* Col-0 seeds were sown at the four corners of the boxes
170 and the lids closed. Plants were grown in a growth cabinet under short-day conditions (day:
171 22 °C, 10 h light; 70% humidity) for 4.5 weeks. Then, plants were inoculated with *G. orontii*
172 under sterile conditions (n=6, no SynCom culture, and n=6, previously treated with SynCom
173 culture). In addition, some boxes that were either mock- or SynCom-inoculated were opened,
174 but not inoculated with *G. orontii,* serving as a control. At 11 dpi, root and leaf tissues were
175 harvested (Figure 4a).

176 For the leaf SynCom, 70 mL ½ MS media (including vitamins without sucrose, pH 7, Sigma-
177 Aldrich GmbH, CatNo M5524-1L) were mixed into the calcined-clay-containing magenta
178 boxes, and surface-sterilized *A. thaliana* seeds sown at the four corners of the boxes. Plants
179 were grown in a growth cabinet under short-day conditions (day: 21 °C, 10 h light; night: 19
180 °C; 70% humidity) for 3.5 weeks. Then, a 10-fold dilution of the leaf SynCom in 10 mM $MgCl_2$
181 was used to spray five times with a Reagent Sprayer (CAMAG®Glass Reagent Spray, Muttenz,
182 Switzerland) onto the *A. thaliana* plants (see (Bai *et al.*, 2015); here*:* 1 spray volume = approx.
183 35 µL; n=18). At 14 d after the addition of the SynCom or respective mock treatments, plants
184 were inoculated with *G. orontii* under sterile conditions (n=5, no SynCom, and n=9, previously
185 treated with SynCom culture). In addition, some boxes that were either mock- or SynCom-
186 inoculated were opened, but not inoculated with *G. orontii,* serving as a control. At 7 dpi, root
187 and leaf tissues were harvested (Figure 4a).

188 **Microbial profiling from plant tissues**

189 Total DNA was extracted from the samples mentioned above using the FastDNA SPIN Kit for
190 Soil (MP Biomedicals, Solon, USA). Samples were homogenized in Lysis Matrix E tubes (MP

191 Biomedicals, Heidelberg, Germany) using the Precellys 24 tissue lyzer (Bertin Technologies,
192 Montigny-le-Bretonneux, France) at 6200 rpm for 30 s. DNA samples were then eluted in
193 80 µL nuclease-free water and used for bacterial and fungal community profiling (Durán *et*
194 *al.*, 2018). Concentrations of DNA samples were fluorescently quantified, adjusted to
195 3.5 ng/µL, and samples used as templates in a two-step PCR amplification protocol. In the
196 first step, the V5–V7 region of bacterial *16S* rRNA (primers 799F-1192R), fungal *ITS1* (primers
197 ITS1F-ITS2) and *ITS2* (primers fITS7-ITS4) regions were amplified. Under a sterile hood, each
198 sample was amplified in triplicate in a 25 µL reaction volume containing 2 U DFS-Taq DNA
199 polymerase, 1x incomplete buffer (both Bioron GmbH, Ludwigshafen, Germany), 2 mM
200 $MgCl_2$, 0.3% BSA, 0.2 mM dNTPs (Life Technologies GmbH, Darmstadt, Germany) and 0.3 µM
201 forward and reverse primers. PCR was performed using the same parameters for all primer
202 pairs (94 °C/2 min, 94 °C/30 s, 55 °C/30 s, 72 °C/30 s, 72 °C/10 min for 25 cycles).
203 Afterwards, single-stranded DNA and proteins were digested by adding 1 µL of
204 Antarctic phosphatase, 1 µL xonuclease I and 2.44 µL Antarctic Phosphatase buffer (New
205 England BioLabs GmbH, Frankfurt, Germany) to 20 µL of the pooled PCR product. Samples
206 were incubated at 37 °C for 30 min and subsequently enzymes deactivated at 85 °C for
207 15 min. Samples were then centrifuged for 10 min at 4000 rpm, and 3 µL of this reaction were
208 used for a second PCR, prepared in the same way as described above, using the same
209 amplification protocol but with the number of cycles reduced to 10, and with primers
210 including barcodes with Illumina adaptors (Table S1). PCR product quality was controlled by
211 loading 5 µL of each reaction on an agarose gel and affirming that no band was detected in
212 the negative control. Afterwards, the replicated reactions were combined and purified as
213 follows: Bacterial amplicons were loaded on a 1.5 % agarose gel and run for 2 h at 80 V; bands
214 with the correct size of ~500 bp were cut out and purified using the QIAquick gel
215 extraction kit (Qiagen GmbH, Hilden, Germany). Fungal amplicons were purified using
216 Agencourt AMPure XP beads (Thermo Fisher Scientific). DNA concentration was again
217 fluorescently determined, and 30 ng DNA of each of the barcoded amplicons were pooled in
218 one library per microbial group. Each library was then purified and re-concentrated twice
219 with Agencourt AMPure XP beads, and 100 ng of each library were pooled together. Paired-
220 end Illumina sequencing was performed in-house using the MiSeq sequencer and custom
221 sequencing primers (Table S1).

222 **Absolute quantification of microbial load in plant tissues**

223 Genomic DNA from leaves inoculated with SynCom alone (n=9), *G. orontii* alone (n=9), both
224 SynCom and *G. orontii* (n=9), or mock-treated (n=9) was used for absolute quantification of
225 microbial load. Genomic DNA was fluorescently quantified and diluted to an equal
226 concentration of 4 µL. Each sample was subsequently used for absolute quantification *via* PCR
227 (qPCR) by adding SYBR green to monitor the PCR amplification in real time. Each sample was
228 amplified in duplicate: 4 µL of template were mixed with 7.5 µL of SYBR green (brand),
229 together with 1.2 µL of forward primer and 1.2 µL of reverse primer, to a final volume of 15
230 µL of reaction. For each organism, a specific primer pair was selected: for bacterial
231 assessment, the *16S* rRNA gene (primers 799F-1192R, (Wippel *et al.*, 2021)); for *G. orontii*, a
232 GDSL lipase-like gene (primers R263-R264, (Weßling & Panstruga, 2012)); and, for *A. thaliana*,
233 the *At4G26410* gene (primers L658-L659, (Hong *et al.*, 2010)). The following program was
234 used for amplification: pre-denaturation for 3 min at 94 °C, followed by 40 cycles of
235 denaturation for 15 s at 95 °C, annealing for 10 s at 62 °C and elongation for 10 s at 72 °C.
236 Melting curve analysis was performed from 55 °C to 95 °C, with a step-wise increase of 0.5
237 °C. The amount of bacterial and *G. orontii* genes was normalized to the reference plant gene
238 within each individual sample using the $2^{-\Delta\Delta Ct}$ equation (Pfaffl, 2001). Absolute abundances of
239 individual bacteria in SynCom experiments were obtained by multiplying the bacterial
240 gene/plant gene ratio to their individual relative abundances (RAs).

241 **Processing of *16S* gene and *ITS* region amplicon data**

242 Amplicon sequencing data from the natural soil experiment (plant tissues along with
243 unplanted controls) were demultiplexed according to their barcode sequence using the QIIME
244 pipeline (Caporaso *et al.*, 2010). Afterwards, DADA2 (Callahan *et al.*, 2016) was used to process
245 the raw sequencing reads of each sample. Unique amplicon sequence variants (ASVs) were
246 then inferred from error-corrected reads, followed by chimera filtering, also using the DADA2
247 pipeline. Next, ASVs were aligned to the SILVA database (Quast *et al.*, 2013) for taxonomic
248 assignment using the naïve Bayesian classifier implemented by DADA2. Next, raw reads were
249 mapped to the inferred ASVs to generate an abundance table, which was subsequently
250 employed for analyses of diversity (using the R package vegan, (Oksanen *et al.*, 2007)) and
251 differential abundance using the R package DESeq2 (Love *et al.*, 2014).
252 Sequencing data from SynCom experiments was processed using the Rbec tool (Zhang *et al.*,
253 2021). First, reads were de-replicated into unique tags and subsequently aligned to the
254 reference database, after which initial abundances were assigned to each strain according to

255 the copy number of each exactly aligned tag. Next, tags that were not exactly matched to any
256 sequence in the database were assigned a candidate error-producing reference based on *k*-
257 mer distances. Sequencing reads were then subsampled and an error matrix is calculated using
258 the mapping between subsampled reads and candidate error-producing sequences. The
259 parameters of the error model were recomputed iteratively until the number of re-
260 assignments fell below the set threshold. Strain abundances were then estimated from the
261 number of error-corrected reads mapped to each reference sequence. Next, we generated a
262 count table that was employed for downstream analyses of diversity with the R package vegan
263 (Oksanen *et al.*, 2007). Reads assigned to a given strain were normalized by its *16S* copy
264 number. Finally, amplicon data from all experimental systems were visualized using the
265 ggplot2 R package (Wickham, 2016).

266

267 **Results**

268 ***G. orontii*-induced changes in root- and leaf-derived natural microbial communities**

269 *A. thaliana* plants (accession Col-0) were grown in Cologne agricultural soil (CAS12;
270 (Bulgarelli *et al.*, 2012)) for 6.5 weeks and subsequently rosette leaves inoculated with *G.*
271 *orontii* conidiospores. Samples of leaf, root, and rhizosphere compartments as well as
272 unplanted soil were harvested at 11 dpi (Figure 1A). Genomic DNA was prepared from these
273 samples and used for PCR-based amplification of the bacterial *16S* rRNA genes and the
274 fungal ribosomal internal transcribed spacer (*ITS*) regions, *ITS1* and *ITS2*. PCR amplicons were
275 subjected to Illumina sequencing and the resulting sequencing data used for the analysis of
276 the bacterial and fungal communities in the respective compartments. Information on the
277 number and RA of amplicon sequence variants (ASVs) in each compartment was used to
278 calculate α-diversity (Shannon index; within-sample diversity), β-diversity (Bray-Curtis
279 dissimilarities; between-sample diversity), ASV enrichment, and taxonomic composition.
280 Consistent with previous reports (Bulgarelli *et al.*, 2012; Schlaeppi *et al.*, 2014; Thiergart *et*
281 *al.*, 2020), we found the highest bacterial α-diversity in unplanted soil and the rhizosphere
282 compartment, and lower α-diversity in roots and leaves. There was no significant difference
283 in α-diversity between mock-treated and *G. orontii*-inoculated samples for any of the four
284 compartments analyzed (Figure 1B). By contrast, we observed that in leaves, fungal α-
285 diversity, determined *via ITS1* sequences, was significantly (P=0.05) decreased in *G. orontii*-
286 inoculated leaves (by ca. 70%; Figure 1B). This drop in α-diversity was retained upon *in silico*
287 depletion of *G. orontii* reads, excluding the possibility that the decrease in species richness
288 was due to an overrepresentation of powdery mildew reads (and thus underrepresentation
289 of reads from other fungal taxa) in the samples. A similar outcome was obtained with *ITS2*
290 amplicons (Figure 1B). Together, these findings suggest that *G. orontii* leaf colonization
291 reduces the diversity of leaf-associated fungal communities whereas α-diversity of bacterial
292 assemblages remains unaltered.

293 Analysis of β-diversity using principal-coordinates analysis (PCoA) of Bray-Curtis
294 dissimilarities revealed distinctive community compositions in unplanted soil, rhizosphere,
295 root and leaf compartments (30% of variance explained, P=0.001, Figure 2A). We noted that
296 β-diversity of leaf-associated bacterial assemblages changes in response to *G. orontii*
297 inoculation (P=0.029), whereas bacterial communities remained indistinguishable in the

298 other compartments (Figure 2B and E). This suggests that *G. orontii* exerts a local effect on
299 bacterial community profiles, but not systemically on the bacterial root and/or rhizosphere
300 microbiota. Closer inspection of the *G. orontii*-induced bacterial community shifts in leaves
301 reveals a broad range of bacterial ASVs that show significantly altered RAs (differentially
302 abundant ASVs; $P<0.05$). This shift affects both abundant and low-abundant community
303 members with ASVs that are enriched or depleted (4.4% and 2.5% of differentially abundant
304 ASVs, respectively). The majority of taxa with differential fold changes are either
305 undetectable in the absence of *G. orontii* (enriched taxa) or undetectable following *G. orontii*
306 challenge (depleted taxa; Supplemental Figure 1). Similar to the leaf-associated bacterial
307 commensals, analysis of β-diversity of the leaf-associated fungal community reveals a
308 marked community shift (*ITS1* Figure 2C; *ITS2* Figure 2D). As with the changes in α-diversity
309 (Figure 1B), the differentiation in distinct leaf-associated fungal communities following
310 powdery mildew infection is not due to an overrepresentation of *G. orontii* reads, as
311 indicated by a similar outcome upon *in silico* depletion of the corresponding reads (Figure
312 2E).

313 Permutational multivariate analysis of variance revealed that *G. orontii* leaf colonization
314 explained ca. 15% and ca. 34-45% of the variation of the leaf-associated bacterial or fungal
315 communities, respectively (Figure 2E). To explore the changes driving this variation in
316 community structure, we calculated the proportion of bacterial ASVs with differential
317 abundance upon *G. orontii* infection at the order level. For the majority of bacterial orders
318 with multiple differentially abundant ASVs, both enriched and depleted ASVs were found,
319 although we observed more differentially enriched than differentially depleted ASVs. The
320 two orders with the greatest proportion of differentially abundant ASVs were
321 Burkholderiales and Rhizobiales (ca. 33% and 9.5%, respectively; Figure 3A), two abundant
322 bacterial taxa robustly found in *A. thaliana* leaf microbiota (Garrido-Oter *et al.*, 2018). We
323 also tested whether differentially enriched or depleted ASVs for a given bacterial order
324 affect its aggregated RA. Whereas the aggregated RA of Burkholderiales, Flavobacteriales
325 and Rhizobiales increases, the aggregated RA of Pseudonocardiales is reduced upon *G.*
326 *orontii* inoculation ($P<0.05$; Figure 3B). As these four bacterial orders belong to three phyla,
327 Proteobacteria, Actinobacteria and Bacteroidetes, *G. orontii* colonization influences the
328 abundance of phylogenetically distantly related bacterial leaf commensals.

329 Closer inspection of the *G. orontii*-induced fungal community shift showed that a great
330 proportion (15-34%) of taxa were depleted (Supplemental Figure 2), including abundant and
331 low abundant members of a variety of fungal classes. This result is consistent with the
332 aforementioned *G. orontii*-induced reduction in fungal α-diversity (Figure 1B). However, nine
333 fungal taxa are significantly enriched, with members of the Erysiphales and the Golubeviales
334 showing the highest fold change. Besides *G. orontii*, we noticed the presence of other
335 powdery mildew species (*Erysiphe* spp.) among the enriched fungal taxa. These could either
336 be contaminations in our inoculum or species introduced from the environment in the
337 course of the experiment and "hitchhiking" on the diseased plants.

338 In summary, we observed a major shift in the resident fungal community in *G. orontii*-
339 infected leaves, characterized by predominantly depleted taxa compared to non-infected
340 plants. In contrast, changes in the leaf-associated bacterial communities were more limited,
341 with both enriched and depleted taxa. No alterations were seen in the systemic root tissue.

342 ***G. orontii*-induced changes in root- and leaf bacterial SynComs**

343 We examined the impact of *G. orontii* leaf infection using a gnotobiotic *A. thaliana* system
344 and defined *A. thaliana* root and leaf bacterial consortia (root- and leaf-derived *At*-SPHERE
345 strains), which comprise representatives of the majority of taxa that are detectable by
346 culture-independent *16S* rRNA amplicon sequencing in association with plants grown in
347 natural soil (Bai *et al.*, 2015). In this gnotobiotic plant system, *A. thaliana* surface-sterilized
348 seeds were sown on a calcined clay matrix. In the first experiment, we inoculated prior to
349 sowing a defined bacterial consortium consisting of 88 root-derived bacterial commensals
350 (designated here 'root SynCom'), co-cultivated the consortium with the host for 4.5 weeks,
351 followed by either *G. orontii* conidiospore inoculation or mock treatment. At 11 dpi, leaf,
352 matrix and root samples were harvested and the corresponding DNA preparations subjected
353 to *16S* rRNA amplicon sequencing (Figure 4A, upper panel). PCoA of Bray-Curtis
354 dissimilarities of the bacterial consortia revealed their separation according to compartment
355 (12-22% of variance explained, P=0.001, Figure 4B-C). In addition, root-associated consortia
356 were found to be more similar to matrix-associated communities, while still separated from
357 the leaf-resident assemblages (Figure 4B; Supplementary Figure 4). The latter community is
358 likely the result of upward bacterial migration from roots to shoots during co-cultivation
359 (ectopic leaf colonization). In contrast to root samples, leaf samples collected from matrix-

360 inoculated root SynComs differentiated significantly upon *G. orontii* infection (*P*=0.02; Figure
361 4D and G; Supplementary Figure 4). This pattern is reminiscent of the *G. orontii*-induced
362 impact on *A. thaliana* plants grown in natural soil with an infection-induced change in the
363 bacterial leaf microbiota but non-responsiveness of the root-associated community (Figure
364 2F).

365 In the second experiment, *A. thaliana* plants were grown on sterilized calcined clay matrix
366 and at the age of 3.5 weeks we spray-inoculated leaves with a defined bacterial consortium
367 consisting of 103 leaf-derived bacterial commensals (designated here 'leaf SynCom').
368 Fourteen days after plant-bacteria co-cultivation, leaves were either inoculated with *G.*
369 *orontii* conidiospores or mock-treated. At 7 dpi, leaf and root samples were collected and
370 the corresponding microbial DNA preparations subjected to *16S* rRNA gene amplicon
371 sequencing (Figure 4A, lower panel). PCoA of Bray-Curtis dissimilarities of the bacterial
372 consortia shows their separation according to compartments (Figure 4C; Supplementary
373 Figure 5). Closer inspection revealed a significant separation of mock-treated and *G. orontii*-
374 inoculated samples in both roots and leaves (*P*=0.012 and *P*=0.002, respectively; Figure 4E-G;
375 Supplementary Figure 5). The *G. orontii*-induced shift in the leaf-associated bacterial
376 consortium is consistent with the shift of the leaf microbiota observed in *G. orontii*-
377 inoculated plants in natural soil (Figure 2E). However, unlike the absence of a systemic effect
378 on the bacterial root microbiota in natural soil upon leaf powdery mildew infection (Figure
379 2E), the ectopically located leaf SynCom commensals on roots were responsive to *G. orontii*
380 infection in the gnotobiotic plant system (see Discussion).

381 To assess potential changes in absolute abundance of leaf-associated bacterial communities
382 following *G. orontii* infection, we performed qPCR of the corresponding leaf samples with
383 PCR primers specific for bacterial *16S* rRNA and a *G. orontii*-specific gene and normalized
384 against an *A. thaliana*-specific amplicon (see Materials and Methods). Unexpectedly, we
385 found an approximately 2.1-fold increase in bacterial load in *G. orontii*-colonized leaf
386 samples, whereas *G. orontii* biomass on leaves in either the presence or absence of the
387 bacterial SynCom remained unaltered (Figure 5A). This was confirmed using PCoA of
388 absolute bacterial abundances in leaf samples spray-inoculated with the bacterial SynCom in
389 the presence or absence of *G. orontii*, explaining 56% of the observed variation (Figure 5B).
390 The increase in bacterial load in *G. orontii*-treated leaves could be seen across multiple
391 taxonomic classes, prominently in Actinobacteria, Alphaproteobacteria and Flavobacteria

392 (Figure 5C, Supplementary Figure 6 for data of individual SynCom strains). We further took
393 advantage of the *G. orontii*-infected plants in the gnotobiotic system to analyze the
394 composition of our inoculum. Although *G. orontii*, as expected, is the dominant taxum of the
395 inoculum, this revealed the presence of three additional fungal genera, including a known
396 hyperparasite of powdery mildews and another powdery mildew species (*Erysiphe* sp., >6%
397 average aggregated RA; Supplementary Figure 7).

398

399 **Discussion**

400 In this study, we analyzed in *A. thaliana* the influence of powdery mildew (*G. orontii*)
401 infection on leaf- and root-associated natural and synthetic microbial communities in
402 controlled environments (Figure 1A and 4A). For the experiments conducted in natural soil
403 (Figure 1A), we observed no alteration in bacterial α-diversity in all tested compartments
404 (soil, rhizosphere, root and leaf) following powdery mildew challenge, while α-diversity of
405 the foliar fungal community was strongly reduced (Figure 1B). The more pronounced effect
406 seen with the *ITS1* primers compared to the *ITS2* primer pair was probably a consequence of
407 a greater molecular diversity recovered with the former primers (Bazzicalupo et al., 2013).
408 The substantial reduction in α-diversity of the leaf-associated fungal community upon
409 powdery mildew infection is an indication that the invasive pathogen outcompetes many
410 resident fungal leaf endophytes (15-31% of ASVs), e.g. due to a powdery mildew pathogen-
411 induced shift in sink-source relationships in infected compared to pathogen-free leaves.
412 During a compatible powdery mildew interaction, photosynthetic activity of the plant host is
413 progressively reduced both in cells directly below fungal colonies and in adjacent cells, and
414 this process is associated with an increase in apoplastic invertase activity and an
415 accumulation of hexoses thought to favour pathogen nutrition (Wright et al., 1995;
416 Swarbrick et al., 2006; Eichmann & Hückelhoven, 2008). Alternative explanations may
417 include fungus-specific antibiosis by *G. orontii* or activation of plant immune responses by
418 the fungal invader. The former explanation appears unlikely because the obligate biotrophic
419 pathogen has an unusually low genomic capacity for the biosynthesis of specialized
420 metabolites (Spanu et al., 2010). *G. orontii* pathogenesis stimulates in leaves the
421 accumulation of the defense hormone salicylic acid (SA) at later stages of infection (four dpi)
422 and SA-dependent defense signaling limits hyphal growth and pathogen reproduction
423 (Dewdney *et al.*, 2000; Stein *et al.*, 2008; Poraty-Gavra *et al.*, 2013). For this reason, we
424 consider it plausible that the dramatic reduction in α-diversity of the resident community of
425 asymptomatic leaf-associated fungi in response to *G. orontii* invasion is linked to pathogen-
426 induced and SA-dependent immune responses and/or change in metabolic sink-source
427 relationships. We can, however, not rule out that powdery mildew pathogens deploy
428 secreted effector proteins to antagonize resident endophytic fungi that compete for the
429 same ecological niche (Snelders *et al.*, 2018). Potentially different metabolic demands of
430 leaf-associated commensal bacteria compared to fungi together with the ASV-level

431 compensatory changes seen within numerous bacterial orders of the leaf microbiota could
432 explain why the *G. orontii*-induced shift in nutrient availability and immune status does not
433 affect bacterial commensal diversity in the same way.

434 Consistent with a strong decrease in fungal species richness on *G. orontii*-infected leaves of
435 plants grown in natural soil, we found that the altered fungal community profile is
436 characterized by a reduction in RAs for most and an increase in RAs of a few taxa, while the
437 local bacterial community profile was only slightly affected (Figure 2; Supplementary Figure
438 3). Leaf-associated fungal endophytes whose RA increases upon *G. orontii* infection comprise
439 mainly one other powdery mildew species (*Erysiphe* sp.) or fungi typically associated with
440 them, such as *Golubevia* sp., which are basidiomycete hyperparasites of powdery mildew
441 pathogens (Russ *et al.*, 2021).

442 Closer inspection of the *G. orontii*-induced shift of bacterial community diversity in leaves
443 revealed 40 bacterial orders, containing several ASVs whose RA is depleted or enriched
444 (Figure 3A and Supplemental Figure 1). However, significant alterations in aggregated ASV-
445 level RAs were seen only in four bacterial orders, with three of them showing an increase
446 and one a decrease (Burkholderiales, Flavobacteriales, Rhizobiales and Pseudonocardiales,
447 respectively; Figure 3B). This pattern suggests widespread compensatory changes at the ASV
448 level within bacterial orders that may allow maintenance of the higher taxonomic structure
449 of the bacterial leaf microbiota during powdery mildew pathogenesis. The fungal pathogen
450 thus mediates local community shifts in the aggregated RAs limited to four bacterial orders
451 belonging to the three main phyla of the *A. thaliana* microbiota (Actinobacteria,
452 Proteobacteria and Bacteriodetes (Bulgarelli *et al.*, 2012)). In addition, in our SynCom
453 experiments, colonization by the biotrophic pathogen unexpectedly increased the load of
454 bacterial commensals in leaves approximately 2.1-fold, and this increase was seen roughly
455 equally proportional for all bacterial classes analyzed (Figure 5). The rise in bacterial
456 numbers could be an indirect consequence of the altered sink-source relationships upon
457 infection with the biotrophic pathogen, which turns infected leaves into a metabolic sink
458 associated with an altered availability of non-structural carbohydrates (Wright *et al.*, 1995;
459 Swarbrick *et al.*, 2006). Consequently, the bacterial commensals might benefit from an
460 accumulation and/or alteration in fluxes of apoplastic hexose sugars and reduction in export
461 of sucrose from the leaf.

462 In the case of bacteria, changes were only detectable locally (in the infected leaves) but not
463 systemically (in roots or rhizosphere compartments) and only applied to community
464 diversity, while species richness remains unaltered (Figure 1B and 2). The subtle shift in local
465 bacterial diversity could be an indirect consequence of the significant alterations in fungal
466 community richness and diversity upon *G. orontii* invasion. However, at the bacterial order
467 level, we noted a striking overall similarity of the *G. orontii*-induced local bacterial
468 community shifts between the natural soil and bacterial SynCom experiments (significant
469 increases in the RA of Burkholderiales, Flavobacteriales and Rhizobiales and a similar trend
470 for Caulobacterales; Supplementary Fig. 6B). This suggests that our gnotobiotic plant system
471 recapitulates features of the powdery mildew pathogen-induced bacterial community shifts
472 seen in plants grown in natural soil. It further rules out the possibility that these shifts are
473 the result of bacterial immigration into vacated leaf niches that had to be abandoned by the
474 resident fungal endophytes in the course of *G. orontii* pathogenesis.

475 The only systemic effect on root-associated microbes upon powdery mildew infection
476 reported so far involves nitrogen-fixing rhizobia, which engage in root symbiosis with
477 legumes. In pea (*Pisum sativum*), powdery mildew (*Erysiphe pisi*) colonization was found to
478 result in both a reduction of nodulation and reduced size of root nodules in the leaf-infected
479 plants (Singh & Mishra, 1992). The absence of a systemic effect on the bacterial root
480 microbiota following *G. orontii* challenge differs from *A. thaliana* plants infected with the
481 foliar downy mildew pathogen, the obligate biotrophic oomycete *H. arabidopsidis*.
482 Colonization of leaves with *H. arabidopsidis* promotes the specific enrichment of three
483 bacterial taxa (*Xanthomonas*, *Stenotrophomonas* and *Microbacterium* spp.) from soil to the
484 rhizosphere, where these three taxa synergistically induced systemic defence responses and
485 promoted plant growth, resulting in enhanced disease resistance against downy mildew
486 (Berendsen *et al.*, 2018). Although *G. orontii* and *H. aribidopsidis* are both obligate biotrophic
487 foliar pathogens, only the latter pathogen can infect leaf mesophyll cells and ramify inside
488 this organ, and this may be one reason why only *H. arabidopsidis* can systemically induce
489 changes in the bacterial root microbiota.

490 Our experiments using germ-free plants, pre-inoculated with a root- or a leaf-SynCom and
491 either mock-treated or challenged with *G. orontii* (Figure 4), recapitulated in parts the
492 pathogen-induced shift in bacterial community profiles of plants grown in natural soil.
493 However, in these experiments also the root samples showed a significant difference in β-

494 diversity of the bacterial root microbiota following *G. orontii* inoculation (Figure 4F and G).
495 As roots were not pre-inoculated in this experiment, the bacteria recovered from root
496 samples must have originated from the leaf inoculation and either reached the below-
497 ground roots in calcined clay accidentally (e.g. by wash-off) or by downward migration, e.g.
498 *via* the plant vasculature. Irrespective of the mechanism(s) underlying ectopic root
499 colonization of the leaf-inoculated bacterial SynCom, this result indicates a (subtle) systemic
500 effect of foliar inoculation with the powdery mildew pathogen on the root-associated
501 bacterial community, which was not seen in the experiment with plants grown in natural soil
502 (see above and Figure 2B). This difference is probably the result of different conditions in the
503 two experimental setups. The SynCom experiment involves a reduced complexity of the
504 bacterial community, allowing us to track the RA of many members with strain-specific
505 resolution rather than the RA of ASVs, which could represent an average of multiple
506 genetically polymorphic strains that share an identical *16S* rRNA gene. Therefore, the higher
507 complexity of the root microbiota in natural soil may mask putative systemic effects on
508 bacterial assemblages induced by *G. orontii* colonization.

509 It is surprising that the pre-inoculated leaf SynCom does not mediate detectable protective
510 activity against the fungal powdery mildew pathogen, e.g. through activation of defence-
511 associated gene expression in leaves or antagonistic bacteria-fungus interactions (Figure 5A;
512 (Vogel *et al.*, 2016; Durán *et al.*, 2018)). In roots, the presence of the bacterial microbiota is
513 essential for indirect protection and survival of *A. thaliana* against the otherwise detrimental
514 activity of diverse fungal root endophytes (Durán *et al.*, 2018). In *A. thaliana* leaves, several
515 members of the genus *Sphingomonas*, originally isolated from plants, conferred plant
516 protection against the foliar bacterial pathogen *P. syringae* DC3000 and *Xanthomonas*
517 *campestris* in a gnotobiotic system, whereas no protection was observed by colonization
518 with members of the genus *Methylobacterium* (Innerebner *et al.*, 2011). Thus, our results
519 suggest that the bulk of the resident bacterial leaf microbiota of *A. thaliana* does not have a
520 dedicated role in indirect protection against epiphytic *G. orontii* invasion in the tested
521 gnotobiotic system. Whether this is also true for fungal leaf pathogens that colonize
522 mesophyll cells in the leaf interior remains to be tested.

523 Part of the powdery mildew-induced changes in the *A. thaliana* microbiota could be due to
524 the suppression of plant immunity and reprogramming of host cells for parasitism by the
525 obligate biotrophic pathogen (Schulze-Lefert & Panstruga, 2003). The effect of defence

526 suppression in colonized and neighboring leaf epidermal cells is for example evident by the
527 phenomenon of “induced accessibility”, which refers to enabled host cell entry of non-
528 adapted powdery mildews in the vicinity of established powdery mildew infection sites
529 (Yamaoka *et al.*, 1994; Lyngkjær & Carver, 1999b; Lyngkjær & Carver, 1999a; Lyngkjær *et al.*,
530 2001). Powdery mildew-induced alterations of the host transcriptome likely represent the
531 net outcome of counteracting activities of the plant immune system and the fungal intruder
532 (Fabro *et al.*, 2008). Although leaf-associated bacterial commensals also extensively
533 reprogram host transcriptomes, stimulating and/or repressing the activity of gene clusters
534 enriched in immunity-and metabolism-associated functions in leaves (Vogel *et al.*, 2016), the
535 additional pathogen-specific changes in the host transcriptional profile during infection likely
536 contribute to modulating the quantity and composition of the resident microbiota.

537 Based on the analysis of our *G. orontii* inoculum on gnotobiotic plants, we noted that
538 approximately 50% of the reads originate from different fungi, including a powdery mildew
539 hyperparasite and another powdery mildew species (*Erysiphe* sp.; Supplementary Figure 7).
540 Our finding highlights the difficulties of maintaining a plant pathogen with an obligate
541 biotrophic lifestyle that must be propagated on living host plants in pure culture. The co-
542 occurrence with these microbes may balance powdery mildew proliferation. These
543 observations might have implications not only for the interpretation of aspects of the data
544 obtained in this work, but also for studies that use other obligate biotrophic plant
545 pathogens.

546

Author contributions

PSL and RP conceived the project. RP, PSL and RGO designed the experiments. ALR, AR and HM performed the experiments with natural soil. ALR, AR and PD performed the SynCom experiments. PD and RGO analyzed the data. PD and RGO created the Figures. RP and PSL wrote the manuscript with support from AR, PD and RGO.

Data availability statement

Raw demultiplexed sequencing data and corresponding mapping files will be available at ENA accession number PRJEB43139.

Funding

This research was funded by the Deutsche Forschungsgemeinschaft (DFG, German Research Foundation) under Germany's Excellence Strategy—EXC-number 2048/1—project 390686111 (R.G.-O. and P.S.-L.), the Priority Programme SPP 2125 DECRyPT (R.G.-O. and P.S.-L.), a European Research Council advanced grant (ROOTMICROBIOTA), a RIKEN grant (SYMBIOLOGY), and a cooperative research project with Dong-A University funded by the Republic of Korea to P.S.-L., as well as funds to P.S.-L. from the Max Planck Society. M.H. was supported by JSPS KAKENHI grants 20K05955, 19KT0033 and 15J04093.

566 **References**

567 **Acevedo-Garcia, J, Gruner, K, Reinstädler, A, Kemen, A, Kemen, E, Cao, L, Takken, FLW,**
568 **Reitz, MU, Schäfer, P, O'Connell, RJ, Kusch, S, Kuhn, H, Panstruga, R. 2017.** The powdery
569 mildew-resistant Arabidopsis *mlo2 mlo6 mlo12* triple mutant displays altered infection
570 phenotypes with diverse types of phytopathogens. *Scientific Reports* **7**: 27.
571 **Agler, MT, Ruhe, J, Kroll, S, Morhenn, C, Kim, S-T, Weigel, D, Kemen, EM. 2016.** Microbial
572 hub taxa link host and abiotic factors to plant microbiome variation. *PLoS Biology* **14**:
573 e1002352.
574 **Bai, Y, Müller, DB, Srinivas, G, Garrido-Oter, R, Potthoff, E, Rott, M, Dombrowski, N,**
575 **Munch, PC, Spaepen, S, Remus-Emsermann, M, Huttel, B, McHardy, AC, Vorholt, JA,**
576 **Schulze-Lefert, P. 2015.** Functional overlap of the *Arabidopsis* leaf and root microbiota.
577 *Nature* **528**: 364–369.
578 **Bazzicalupo, AL, Bálint, M, Schmitt, I. 2013.** Comparison of ITS1 and ITS2 rDNA in 454
579 sequencing of hyperdiverse fungal communities. *Fungal Ecology* **6**: 102–109.
580 **Berendsen, RL, Vismans, G, Yu, K, Song, Y, Jonge, R** de, **Burgman, WP, Burmølle, M,**
581 **Herschend, J, Bakker, PAHM, Pieterse, CMJ. 2018.** Disease-induced assemblage of a
582 plant-beneficial bacterial consortium. *ISME Journal*.
583 **Bulgarelli, D, Rott, M, Schlaeppi, K, Ver Loren van Themaat, E, Ahmadinejad, N, Assenza, F,**
584 **Rauf, P, Huettel, B, Reinhardt, R, Schmelzer, E, Peplies, J, Gloeckner, FO, Amann, R,**
585 **Eickhorst, T, Schulze-Lefert, P. 2012.** Revealing structure and assembly cues for
586 *Arabidopsis* root-inhabiting bacterial microbiota. *Nature* **488**: 91–95.
587 **Bulgarelli, D, Schlaeppi, K, Spaepen, S, Ver Loren Themaat, E, Schulze-Lefert, P. 2013.**
588 Structure and functions of the bacterial microbiota of plants. *Annual Review of Plant*
589 *Biology* **64**: 807–838.
590 **Callahan, BJ, McMurdie, PJ, Rosen, MJ, Han, AW, Johnson, AJA, Holmes, SP. 2016.** DADA2:
591 High-resolution sample inference from Illumina amplicon data. *Nature Methods* **13**: 581–
592 583.
593 **Caporaso, JG, Kuczynski, J, Stombaugh, J, Bittinger, K, Bushman, FD, Costello, EK, Fierer, N,**
594 **Peña, AG, Goodrich, JK, Gordon, JI, Huttley, GA, Kelley, ST, Knights, D, Koenig, JE, Ley,**
595 **RE, Lozupone, CA, McDonald, D, Muegge, BD, Pirrung, M, Reeder, J, Sevinsky, JR,**
596 **Turnbaugh, PJ, Walters, WA, Widmann, J, Yatsunenko, T, Zaneveld, J, Knight, R. 2010.**
597 QIIME allows analysis of high-throughput community sequencing data. *Nature Methods* **7**:
598 335–336.
599 **Coleman-Derr, D, Desgarennes, D, Fonseca-Garcia, C, Gross, S, Clingenpeel, S, Woyke, T,**
600 **North, G, Visel, A, Partida-Martinez, LP, Tringe, SG. 2016.** Plant compartment and
601 biogeography affect microbiome composition in cultivated and native Agave species. *New*
602 *Phytologist* **209**: 798–811.
603 **Durán, P, Thiergart, T, Garrido-Oter, R, Agler, M, Kemen, E, Schulze-Lefert, P, Hacquard, S.**
604 **2018.** Microbial interkingdom interactions in roots promote Arabidopsis survival. *Cell* **175**:
605 973-983.e14.
606 **Fabro, G, Di Rienzo, JA, Voigt, CA, Savchenko, T, Dehesh, K, Somerville, S, Alvarez, ME.**
607 **2008.** Genome-wide expression profiling Arabidopsis at the stage of *Golovinomyces*
608 *cichoracearum* haustorium formation. *Plant Physiology* **146**: 1421–1439.

609 **Finkel, OM, Castrillo, G, Herrera Paredes, S, Salas González, I, Dangl, JL. 2017.**
610 Understanding and exploiting plant beneficial microbes. *Current Opinion in Plant Biology*
611 **38**: 155–163.
612 **Gao, C, Montoya, L, Xu, L, Madera, M, Hollingsworth, J, Purdom, E, Singan, V, Vogel, J,**
613 **Hutmacher, RB, Dahlberg, JA, Coleman-Derr, D, Lemaux, PG, Taylor, JW. 2020.** Fungal
614 community assembly in drought-stressed sorghum shows stochasticity, selection, and
615 universal ecological dynamics. *Nature Communications* **11**: 34.
616 **Garrido-Oter, R, Nakano, RT, Dombrowski, N, Ma, K-W, McHardy, AC, Schulze-Lefert, P.**
617 **2018.** Modular traits of the rhizobiales root microbiota and their evolutionary relationship
618 with symbiotic rhizobia. *Cell Host & Microbe* **24**: 155-167.e5.
619 **Hacquard, S, Garrido-Oter, R, González, A, Spaepen, S, Ackermann, G, Lebeis, S, McHardy,**
620 **AC, Dangl, JL, Knight, R, Ley, R, Schulze-Lefert, P. 2015.** Microbiota and host nutrition
621 across plant and animal kingdoms. *Cell Host & Microbe* **17**: 603–616.
622 **Hacquard, S, Schadt, CW. 2015.** Towards a holistic understanding of the beneficial
623 interactions across the *Populus* microbiome. *New Phytologist* **205**: 1424–1430.
624 **Harbort, CJ, Hashimoto, M, Inoue, H, Niu, Y, Guan, R, Rombolà, AD, Kopriva, S, Voges,**
625 **MJEEE, Sattely, ES, Garrido-Oter, R, Schulze-Lefert, P. 2020.** Root-secreted coumarins and
626 the microbiota interact to improve iron nutrition in *Arabidopsis*. *Cell Host & Microbe* **28**:
627 825–837.e6.
628 **Hong, SM, Bahn, SC, Lyu, A, Jung, HS, Ahn, JH. 2010.** Identification and testing of superior
629 reference genes for a starting pool of transcript normalization in Arabidopsis. *Plant and*
630 *Cell Physiology* **51**: 1694–1706.
631 **Innerebner, G, Knief, C, Vorholt, JA. 2011.** Protection of *Arabidopsis thaliana* against leaf-
632 pathogenic *Pseudomonas syringae* by *Sphingomonas* strains in a controlled model system.
633 *Applied and Environmental Microbiology* **77**: 3202–3210.
634 **Jakuschkin, B, Fievet, V, Schwaller, L, Fort, T, Robin, C, Vacher, C. 2016.** Deciphering the
635 pathobiome: Intra- and interkingdom interactions involving the pathogen *Erysiphe*
636 *alphitoides*. *Microbial Ecology* **72**: 870–880.
637 **Lauber, CL, Hamady, M, Knight, R, Fierer, N. 2009.** Pyrosequencing-based assessment of soil
638 pH as a predictor of soil bacterial community structure at the continental scale. *Applied*
639 *and Environmental Microbiology* **75**: 5111–5120.
640 **Lebeis, SL, Paredes, SH, Lundberg, DS, Breakfield, N, Gehring, J, McDonald, M, Malfatti, S,**
641 **Glavina del Rio, T, Jones, CD, Tringe, SG, Dangl, JL. 2015.** Salicylic acid modulates
642 colonization of the root microbiome by specific bacterial taxa. *Science* **349**: 860–864.
643 **Love, MI, Huber, W, Anders, S. 2014.** Moderated estimation of fold change and dispersion
644 for RNA-seq data with DESeq2. *Genome Biology* **15**: 550.
645 **Lundberg, DS, Lebeis, SL, Paredes, SH, Yourstone, S, Gehring, J, Malfatti, S, Tremblay, J,**
646 **Engelbrektson, A, Kunin, V, Del Rio, TG, Edgar, RC, Eickhorst, T, Ley, RE, Hugenholtz, P,**
647 **Tringe, SG, Dangl, JL. 2012.** Defining the core *Arabidopsis thaliana* root microbiome.
648 *Nature* **488**: 86–90.
649 **Lyngkjær, HF, Carver, TLW. 1999a.** Modification of *mlo5* resistance to *Blumeria graminis*
650 attack in barley as a consequence of induced accessibility and inaccessibility. *Physiological*
651 *and Molecular Plant Pathology* **55**: 163–174.

652 **Lyngkjær, MF, Carver, TLW. 1999b.** Induced accessibility and inaccessibility to *Blumeria*
653 *graminis* f.sp *hordei* in barley epidermal cells attacked by a compatible isolate.
654 *Physiological and Molecular Plant Pathology* **55**: 151–162.
655 **Lyngkjær, MF, Carver, TLW, Zeyen, RJ. 2001.** Virulent *Blumeria graminis* infection induces
656 penetration susceptibility and suppresses race-specific hypersensitive resistance against
657 avirulent attack in *Mla1*-barley. *Physiological and Molecular Plant Pathology* **59**: 243–256.
658 **Müller, DB, Vogel, C, Bai, Y, Vorholt, JA. 2016.** The plant microbiota: Systems-level insights
659 and perspectives. *Annual Review of Genetics* **50**: 211–234.
660 **Oksanen, J, Kindt, R, Legendre, P, O'Hara, B, Stevens M.H.H., Oksanen, MJ. 2007.** The
661 vegan package: community ecology package. *R package version*.
662 **Panstruga, R, Kuhn, H. 2019.** Mutual interplay between phytopathogenic powdery mildew
663 fungi and other microorganisms. *Molecular Plant Pathology* **20**: 463–470.
664 **Pfaffl, MW. 2001.** A new mathematical model for relative quantification in real-time RT-PCR.
665 *Nucleic Acids Research* **29**: e45.
666 **Quast, C, Pruesse, E, Yilmaz, P, Gerken, J, Schweer, T, Yarza, P, Peplies, J, Glöckner, FO.**
667 **2013.** The SILVA ribosomal RNA gene database project: Improved data processing and
668 web-based tools. *Nucleic Acids Research* **41**: D590-596.
669 **Russ, L, Lombaers-van der Plas, C, Castillo-Russi, JD, Zijlstra, C, Köhl, J. 2021.** Deciphering
670 the modes of action of *Golubevia sp*., an antagonist against the causal agent of powdery
671 mildew in wheat, using an mRNA-based systems approach. *Biological Control* **152**: 104446.
672 **Schlaeppi, K, Dombrowski, N, Oter, RG, van Loren Themaat, E** ver, **Schulze-Lefert, P. 2014.**
673 Quantitative divergence of the bacterial root microbiota in *Arabidopsis thaliana* relatives.
674 *Proceedings of the National Academy of Sciences of the United States of America* **111**:
675 585–592.
676 **Schulze-Lefert, P, Panstruga, R. 2003.** Establishment of biotrophy by parasitic fungi and
677 reprogramming of host cells for disease resistance. *Annual Review of Phytopathology* **41**:
678 641–667.
679 **Singh, UP, Mishra, GD. 1992.** Effect of powdery mildew (*Erysiphe pisi*) on nodulation and
680 nitrogenase activity in pea (*Pisum sativum*). *Plant Pathology* **41**: 262–264.
681 **Snelders, NC, Kettles, GJ, Rudd, JJ, Thomma, BPHJ. 2018.** Plant pathogen effector proteins
682 as manipulators of host microbiomes? *Molecular Plant Pathology* **19**: 257–259.
683 **Swarbrick, PJ, Schulze-Lefert, P, Scholes, JD. 2006.** Metabolic consequences of susceptibility
684 and resistance (race-specific and broad-spectrum) in barley leaves challenged with
685 powdery mildew. *Plant, Cell & Environment* **29**: 1061–1076.
686 **Thiergart, T, Durán, P, Ellis, T, Vannier, N, Garrido-Oter, R, Kemen, E, Roux, F, Alonso-**
687 **Blanco, C, Ågren, J, Schulze-Lefert, P, Hacquard, S. 2020.** Root microbiota assembly and
688 adaptive differentiation among European Arabidopsis populations. *Nature Ecology &*
689 *Evolution* **4**: 122–131.
690 **Vogel, C, Bodenhausen, N, Gruissem, W, Vorholt, JA. 2016.** The Arabidopsis leaf
691 transcriptome reveals distinct but also overlapping responses to colonization by
692 phyllosphere commensals and pathogen infection with impact on plant health. *New*
693 *Phytologist* **212**: 192–207.
694 **Vorholt, JA. 2012.** Microbial life in the phyllosphere. *Nature Reviews Microbiology* **10**: 828–
695 840.

Weßling, R, Panstruga, R. 2012. Rapid quantification of plant-powdery mildew interactions by qPCR and conidiospore counts. *Plant Methods* **8**: 35.

Wickham, H. 2016. ggplot2. Elegant graphics for data analysis. Cham: Springer International Publishing.

Wippel, K, Tao, K, Niu, Y, Zgadzaj, R, Guan, R, Dahms, E, Zhang, P, Jensen, DB, Logemann, E, Radutoiu, S, Schulze-Lefert, P, Garrido-Oter, R. 2021. Host preference and invasiveness of commensals in the *Lotus* and *Arabidopsis* root microbiota. *bioRxiv*.

Wright, DP, Baldwin, BC, Shephard, MC, Scholes, JD. 1995. Source-sink relationships in wheat leaves infected with powdery mildew. I. Alterations in carbohydrate metabolism. *Physiological and Molecular Plant Pathology* **47**: 237–253.

Yamaoka, N, Toyoda, K, Kobayashi, I, Kunoh, H. 1994. Induced accessibility and enhanced inaccessibility at the cellular level in barley coleoptiles .13. Significance of haustorium formation by the pathogen *Erysiphe graminis* for induced accessibility to the non-pathogen *E. pisi* as asessed by nutritional manipulations. *Physiological and Molecular Plant Pathology* **44**: 217–225.

Zhang, J, Liu, Y-X, Zhang, N, Hu, B, Jin, T, Xu, H, Qin, Y, Yan, P, Zhang, X, Guo, X, Hui, J, Cao, S, Wang, X, Wang, C, Wang, H, Qu, B, Fan, G, Yuan, L, Garrido-Oter, R, Chu, C, Bai, Y. 2019a. NRT1.1B is associated with root microbiota composition and nitrogen use in field-grown rice. *Nature Biotechnology* **37**: 676–684.

Zhang, P, Spaepen, S, Bai, Y, Hacquard, S, Garrido-Oter, R. 2021. Reference-based error correction of amplicon sequencing data from synthetic communities. *bioRxiv*.

Zhang, Z, Kong, X, Jin, D, Yu, H, Zhu, X, Su, X, Wang, P, Zhang, R, Jia, M, Deng, Y. 2019b. *Euonymus japonicus* phyllosphere microbiome is significantly changed by powdery mildew. *Archives of Microbiology* **201**: 1099–1109.

Zhang, Z, Luo, L, Tan, X, Kong, X, Yang, J, Wang, D, Zhang, D, Jin, D, Liu, Y. 2018. Pumpkin powdery mildew disease severity influences the fungal diversity of the phyllosphere. *PeerJ* **6**: e4559.

724 **Figure legends**

725 **Figure 1. Analysis of α-diversity including all culture-independent samples (ASV-level**
726 **analysis) for both bacterial and fungal communities**. **A)** Schematic experimental set-up and
727 representative pictures of mock-treated and *G. orontii*-inoculated plants. **B)** Boxplots of
728 within-sample diversity (Shannon index) for each compartment and condition. Significant
729 differences in bacterial community diversity within compartments are marked with an
730 asterisk (Student´s *t*-test, * $P<0.05$; n.s., not significant).

731

732 **Figure 2. Analysis of β-diversity including all culture-independent samples (ASV-level**
733 **analysis), for both bacterial and fungal communities. A)** PCoA plot of Bray-Curtis
734 dissimilarities between bacterial community samples, color-coded by compartment and
735 shaped based on treatment. **B)** Subset of leaf samples where separation between
736 treatments (mock- vs *G. orontii*-treated) can be observed. **C-D)** PCoA plots of fungal
737 communities in leaf samples for *ITS1* (**C**) and *ITS2* (**D**) profiles. **E)** Variance explained of
738 bacterial (left set of columns) and fungal community structure (right set of columns) upon *G.*
739 *orontii* infection. Note that for fungal communities, an *in silico* depletion of *G. orontii*-
740 assigned reads was performed.

741

742 **Figure 3. Analysis of bacterial ASVs significantly affected by *G. orontii* infection on leaves.**
743 **A)** Proportion of ASVs that significantly changed their relative abundance upon infection
744 with *G. orontii*, grouped by order level, in relation to the overall number of ASVs affected. **B)**
745 Log-transformed aggregated relative abundance of each bacterial order shown in **(A)**, which
746 has both enriched and depleted ASVs, compared between mock and *G. orontii*-treated
747 conditions.

748

749 **Figure 4. Analysis of beta-diversity including all Root *At*-SPHERE SynCom samples and all**
750 **Leaf *At*-SPHERE SynCom samples based on relative abundances. A)** Schematic experimental
751 set-up and representative pictures of mock-treated and *G. orontii*-inoculated plants, with
752 and without SynCom. **B)** PCoA of Bray-Curtis distances of all compartment inoculated with
753 Root *At*-SPHERE strains. **C)** PCoA of Bray-Curtis distances of all compartment inoculated with

754 Leaf *At*-SPHERE strains. **D-F)** Subset of leaf **(D and E)** and root samples **(F),** inoculated with
755 either Root *At*-SPHERE strains **(D)** or Leaf *At*-SPHERE strains **(E and F)**, showing the effect on
756 bacterial community structure upon *G. orontii* infection (different shapes). **G)** Variance
757 explained on bacterial community structure upon *G. orontii* infection (PERMANOVA analysis
758 on Bray-Curtis dissimilarities).

759

760 **Figure 5. Absolute quantification of bacterial load on leaves inoculated with Leaf *At*-**
761 **SPHERE strains. A)** Bacterial (left panel) and *G. orontii* (right panel) load calculated as the
762 relative quantification of each microbial gene to an *A. thaliana* reference gene. **B)** PCoA plot
763 of absolute abundances of bacterial communities in leaves inoculated with Leaf *At*-SPHERE
764 strains. **C)** Absolute abundance of each strain utilized in this experiment, color-coded by
765 their taxonomic assignment at the family level, in leaf SynCom-inoculated leaves mock- and
766 *G. orontii*-treated.

767

768 **Supplementary Figure 1: Changes in RA of bacterial ASVs in *A. thaliana* leaves upon *G.***
769 ***orontii* inoculation.** Each bacterial ASV that showed significant enrichment in leaf samples
770 treated with *G. orontii*, compared to mock-treated samples ($P<0.05$, DESeq package in R) is
771 shown. Each row represents a different ASV, where the size of each dot corresponds to the
772 log-transformed RA in a given sample (columns). The dots are color-coded based on the ASV
773 taxonomic assignment at the class level. The right panel depicts the fold change of each
774 significantly enriched ASV in *G. orontii*-treated leaves, compared to mock control.

775

776 **Supplementary Figure 2: Changes in RA of fungal ASVs in *A. thaliana* leaves upon *G. orontii***
777 **inoculation, for the ITS1 community profiles.** Each fungal ASV that showed significant
778 enrichment in leaf samples treated with *G. orontii*, compared to mock-treated samples
779 ($P<0.05$, DESeq package in R) is shown here. Each row represents a different ASV, where the
780 size of each dot corresponds to the log-transformed RA in a given sample (columns). The dots
781 are color-coded based on the ASV taxonomic assignment at the class level. The right panel
782 depicts the fold change of each significantly enriched ASV in *G. orontii*-treated leaves,
783 compared to mock control.

784

785 **Supplementary Figure 3: Changes in RA of fungal ASVs in *A. thaliana* leaves upon *G. orontii***
786 **inoculation, for the ITS2 community profiles.** Each fungal ASV that showed significant
787 enrichment in leaf samples treated with *G. orontii*, compared to mock-treated samples
788 (P<0.05, DESeq package in R) is shown here. Each row represents a different ASV, where the
789 size of each dot corresponds to the log-transformed RA in a given sample (columns). The dots
790 are color-coded based on the ASV taxonomic assignment at the class level. The right panel
791 depicts the fold change of each significantly enriched ASV in *G. orontii*-treated leaves,
792 compared to mock control.

793

794 **Supplementary Figure 4: Heatmap of bacterial strain-specific RA including SynCom samples**
795 **(Root *At*-SPHERE strains).** Warm colors correspond to abundant strains detected in at least
796 one input sample (>0.1% RA). Samples (columns) are grouped by compartment and *G. orontii*
797 treatment.

798

799 **Supplementary Figure 5: Heatmap of bacterial strain-specific RAs including SynCom samples**
800 **(Leaf *At*-SPHERE strains).** Warm colors correspond to abundant strains detected in at least
801 one input sample (>0.1% RA). Samples (columns) are grouped by compartment and *G. orontii*
802 treatment.

803

804 **Supplementary Figure 6: Comparison of absolute abundances of individual Leaf *At*-SPHERE**
805 **bacteria to RAs in the culture-independent approach. A)** Absolute abundance (shown as the
806 product of the bacterial/plant gene ratio multiplied with the bacterial RA of each bacterial
807 strain from the Leaf *At*-SPHERE inoculated in *A. thaliana* leaves without and with *G. orontii*.
808 Boxplots are color-coded based on the taxonomic assignment of each strain at the class level.
809 Significant differences in absolute abundances upon *G. orontii* inoculation are depicted with a
810 red asterisk (Student's *t*-test, P< 0.05, FDR corrected). **B)** Aggregated relative (culture-
811 independent approach) and absolute (culture-dependent approach) abundances of bacterial
812 orders shared between the two experimental set-ups. Significant differences in abundances

813 upon *G. orontii* inoculation are depicted with a red asterisk (Student's *t*-test, $P < 0.05$, FDR
814 corrected).

815

816 **Supplementary Figure 7: Profiling of *G. orontii* inoculum. A)** Number of reads assigned to
817 either bacterial or fungal ASVs in *A. thaliana* leaves inoculated with *G. orontii* **B)** RAs of
818 bacterial ASVs color-coded based on their taxonomic assignment at the class level. **C)** RAs of
819 fungal ASVs from the ITS1 profiles, color-coded based on their taxonomic assignment at the
820 genus level. **D)** RAs of fungal ASVs from the ITS2 profiles, color-coded based on their
821 taxonomic assignment at the genus level.

822

823 **Supplementary Table 1:**

824 - List of Root *At*-SPHERE strains used in this study and their taxonomic assignment
825 - List of Leaf *At*-SPHERE strains used in this study and their taxonomic assignment
826 - Primers used in library preparation for amplicon sequencing
827 - Sequencing primers used for MiSeq sequencing
828 - Natural soil experiment mapping file for the analysis of community profiles
829 - SynCom experiments mapping file for the analysis of community profiles
830 - Primers used in qPCR for microbial absolute quantification in plant tissues

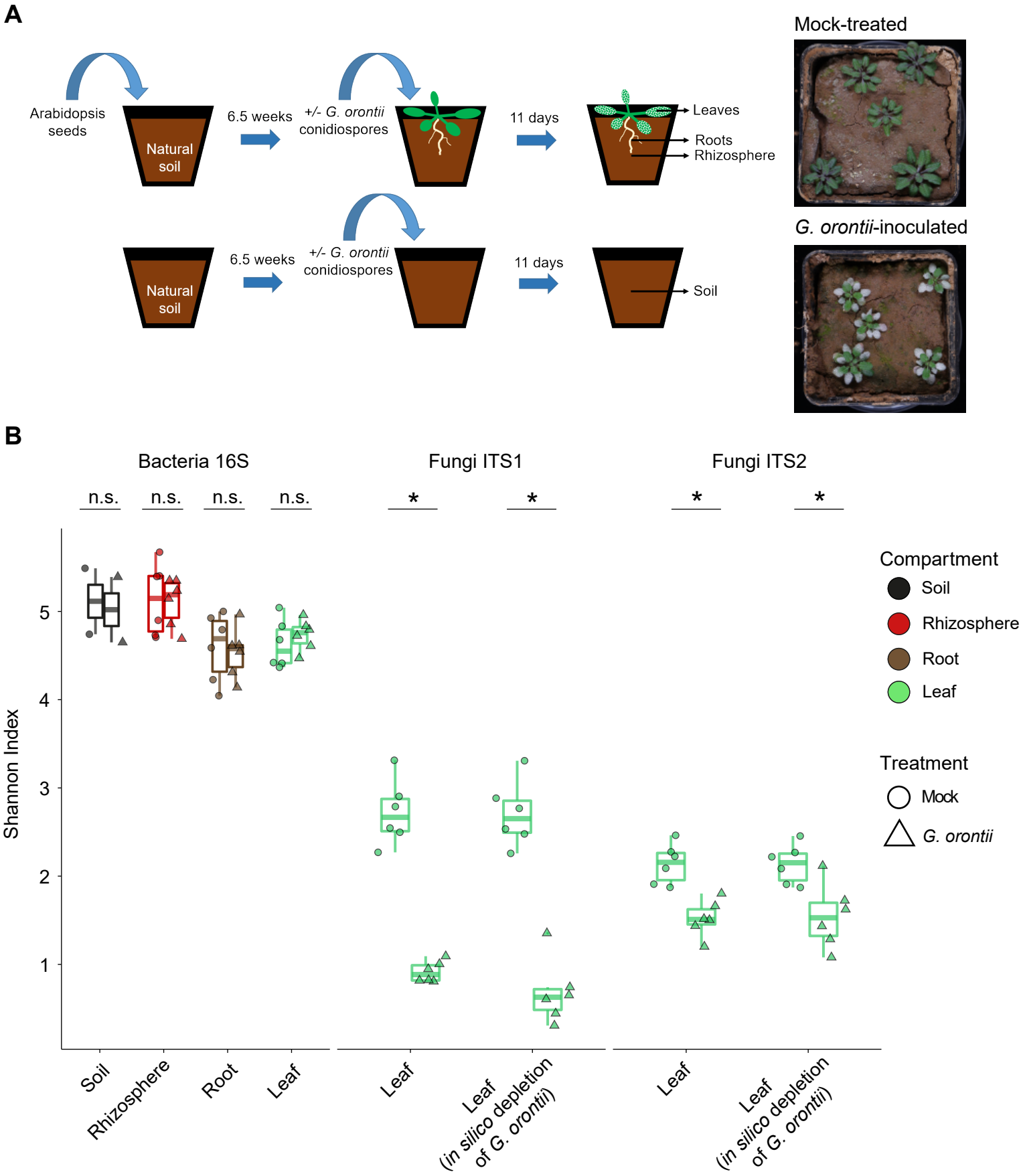
A
Arabidopsis seeds
Natural soil
6.5 weeks
+/- G. orontii conidiospores
11 days
Leaves
Roots
Rhizosphere
Natural soil
6.5 weeks
+/- G. orontii conidiospores
11 days
Soil
Mock-treated
G. orontii-inoculated
B
Bacteria 16S
Fungi ITS1
Fungi ITS2
n.s.
n.s.
n.s.
n.s.
*
*
*
*
Shannon Index
1
2
3
4
5
Soil
Rhizosphere
Root
Leaf
Leaf
Leaf (in silico depletion of G. orontii)
Leaf
Leaf (in silico depletion of G. orontii)
Compartment
Soil
Rhizosphere
Root
Leaf
Treatment
Mock
G. orontii

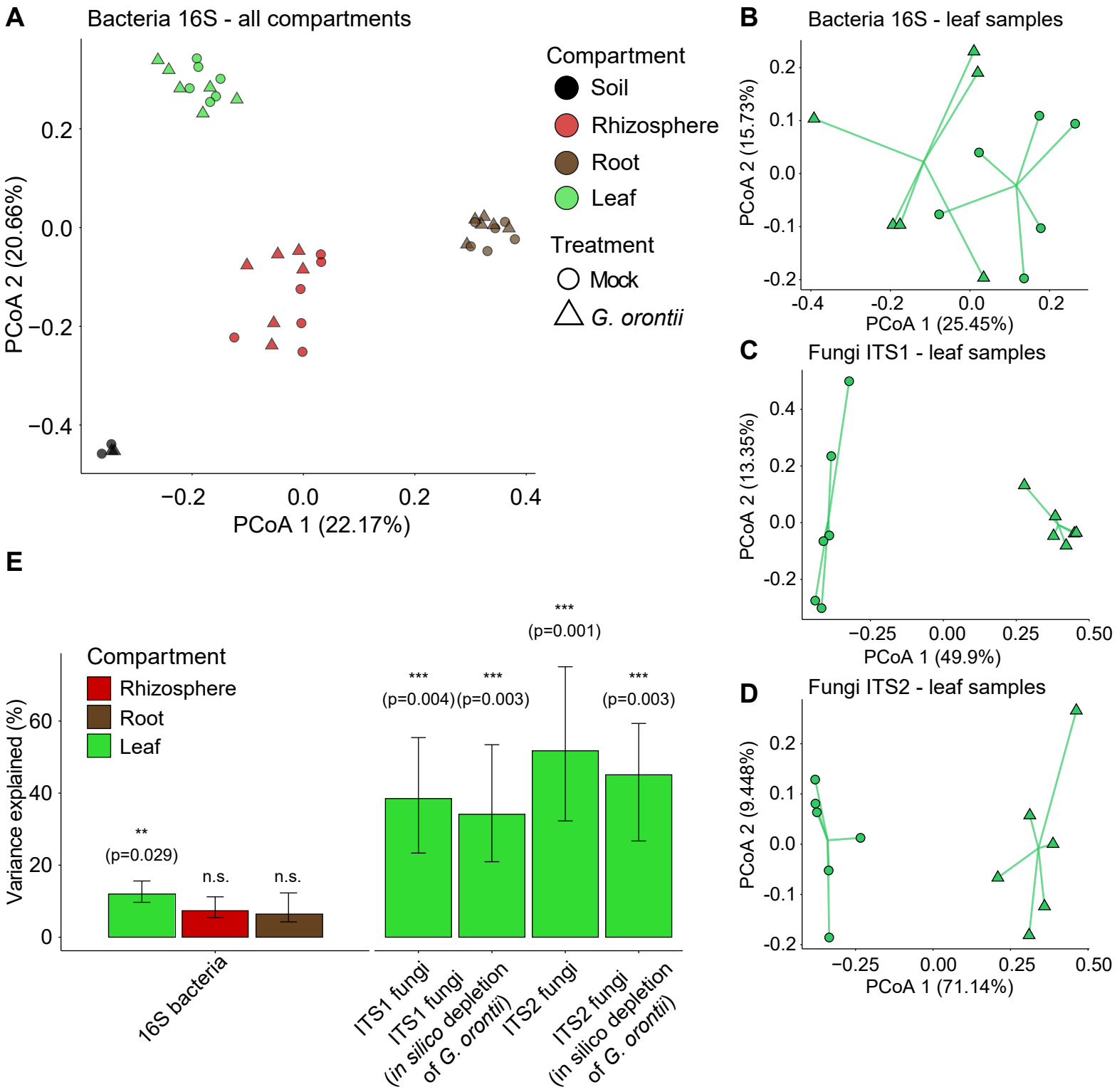
A
Bacteria 16S - all compartments
PCoA 2 (20.66%)
PCoA 1 (22.17%)
Compartment
Soil
Rhizosphere
Root
Leaf
Treatment
Mock
G. orontii
B
Bacteria 16S - leaf samples
PCoA 2 (15.73%)
PCoA 1 (25.45%)
C
Fungi ITS1 - leaf samples
PCoA 2 (13.35%)
PCoA 1 (49.9%)
D
Fungi ITS2 - leaf samples
PCoA 2 (9.448%)
PCoA 1 (71.14%)
E
Compartment
Rhizosphere
Root
Leaf
Variance explained (%)
**
(p=0.029)
n.s.
n.s.
***
(p=0.004)
***
(p=0.003)
***
(p=0.001)
***
(p=0.003)
16S bacteria
ITS1 fungi
ITS1 fungi (in silico depletion of G. orontii)
ITS2 fungi
ITS2 fungi (in silico depletion of G. orontii)

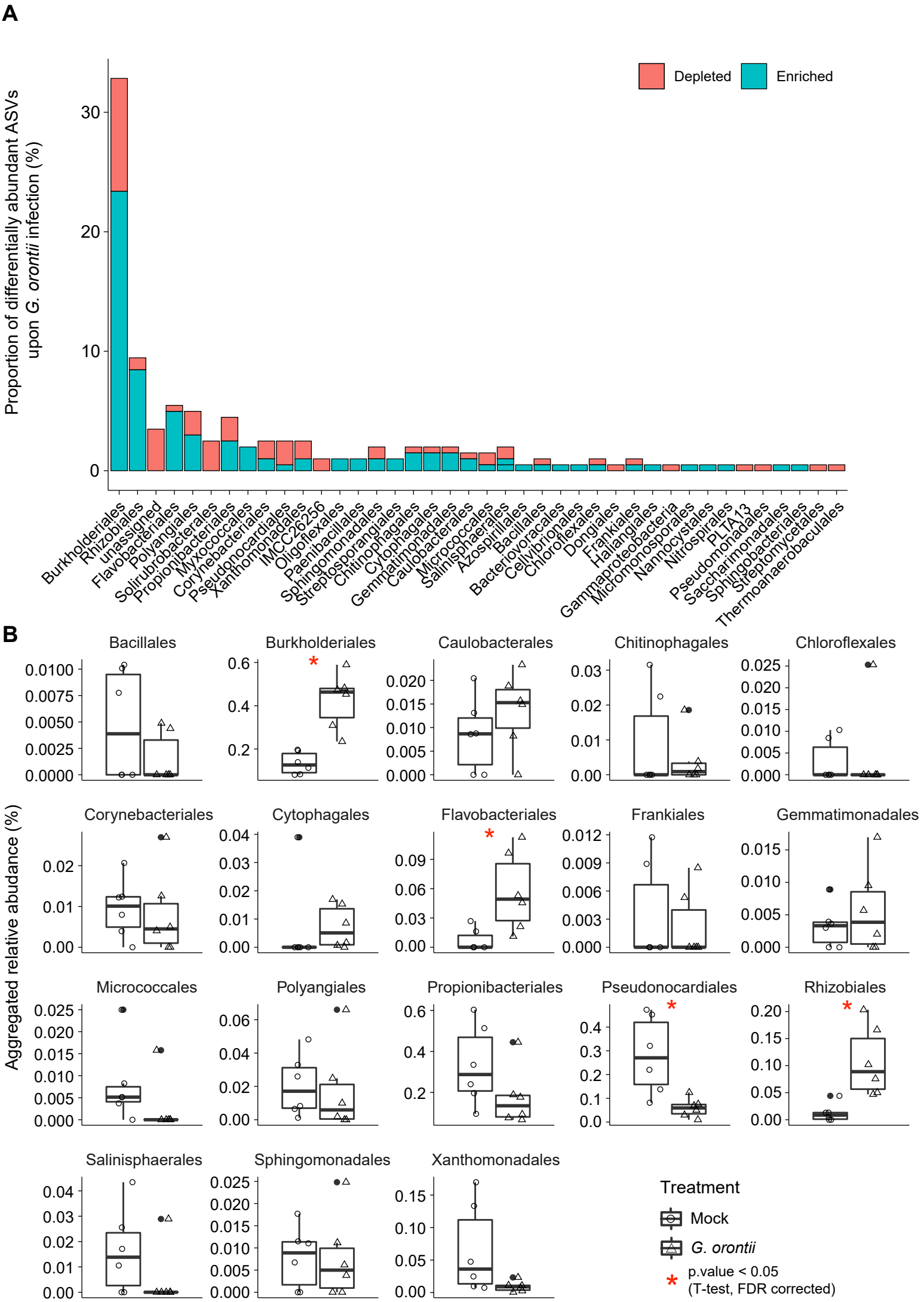
A
Depleted
Enriched
Proportion of differentially abundant ASVs upon G. orontii infection (%)
0
10
20
30
Burkholderiales
Rhizobiales
unassigned
Flavobacteriales
Polyangiales
Solirubrobacterales
Propionibacteriales
Myxococcales
Corynebacteriales
Pseudonocardiales
Xanthomonadales
IMCC26256
Oligoflexales
Paenibacillales
Sphingomonadales
Streptosporangiales
Chitinophagales
Cytophagales
Gemmatimonadales
Caulobacterales
Micrococcales
Salinisphaerales
Azospirillales
Bacillales
Bacteriovoracales
Cellvibrionales
Chloroflexales
Dongiales
Frankiales
Haliangiales
Gammaproteobacteria
Micromonosporales
Nannocystales
Nitrospirales
PLTA13
Pseudomonadales
Saccharimonadales
Sphingobacteriales
Streptomycetales
Thermoanaerobaculales
B
Bacillales
Burkholderiales
Caulobacterales
Chitinophagales
Chloroflexales
Corynebacteriales
Cytophagales
Flavobacteriales
Frankiales
Gemmatimonadales
Micrococcales
Polyangiales
Propionibacteriales
Pseudonocardiales
Rhizobiales
Salinisphaerales
Sphingomonadales
Xanthomonadales
Aggregated relative abudance (%)
Treatment
Mock
G. orontii
p.value < 0.05
(T-test, FDR corrected)

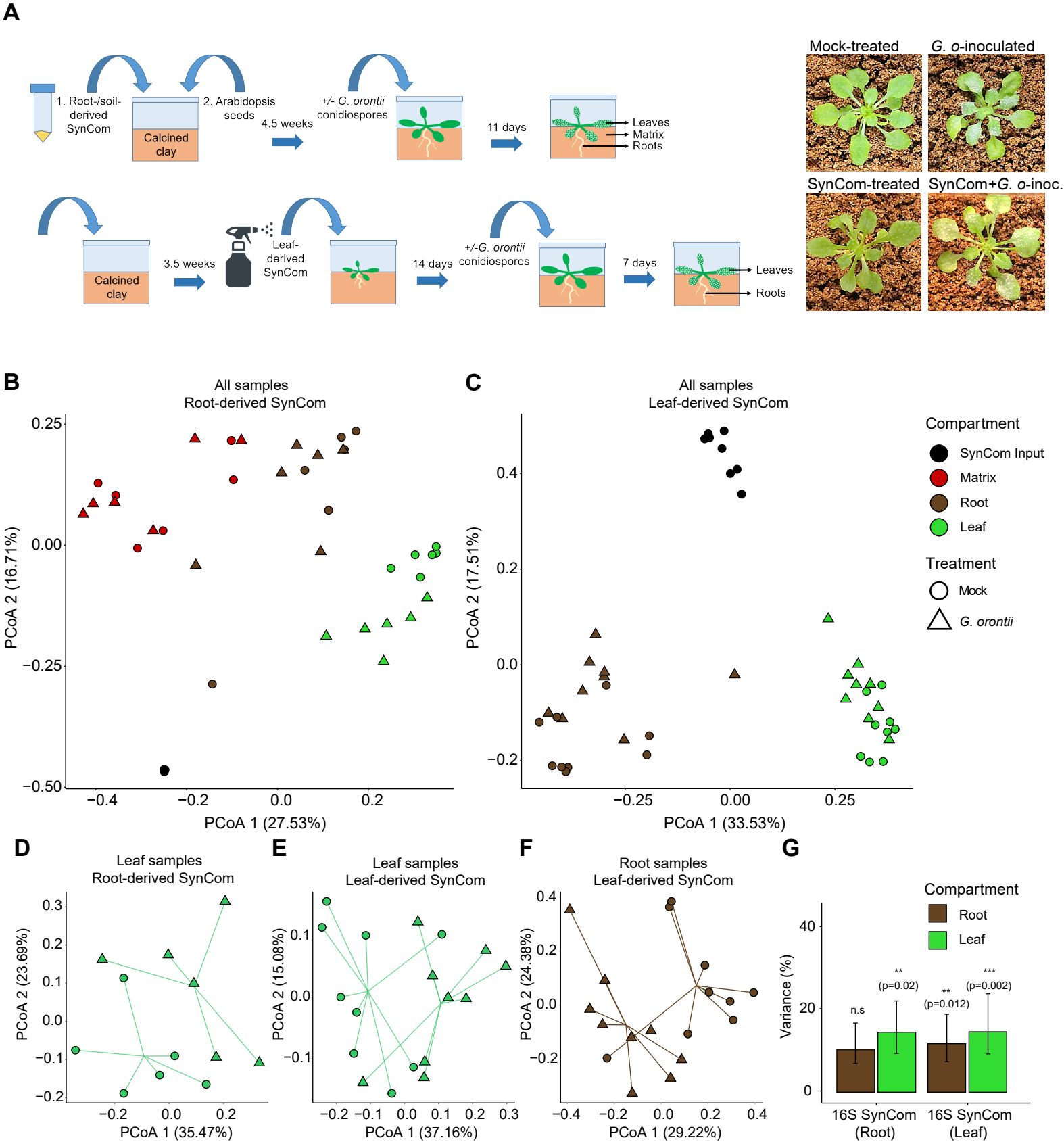
A
1. Root-/soil-derived SynCom
Calcined clay
2. Arabidopsis seeds
4.5 weeks
+/- G. orontii conidiospores
11 days
Leaves
Matrix
Roots
Calcined clay
3.5 weeks
Leaf-derived SynCom
14 days
+/-G. orontii conidiospores
7 days
Leaves
Roots
Mock-treated
G. o-inoculated
SynCom-treated
SynCom+G. o-inoc.
B
All samples
Root-derived SynCom
PCoA 2 (16.71%)
PCoA 1 (27.53%)
C
All samples
Leaf-derived SynCom
PCoA 2 (17.51%)
PCoA 1 (33.53%)
Compartment
SynCom Input
Matrix
Root
Leaf
Treatment
Mock
G. orontii
D
Leaf samples
Root-derived SynCom
PCoA 2 (23.69%)
PCoA 1 (35.47%)
E
Leaf samples
Leaf-derived SynCom
PCoA 2 (15.08%)
PCoA 1 (37.16%)
F
Root samples
Leaf-derived SynCom
PCoA 2 (24.38%)
PCoA 1 (29.22%)
G
Compartment
Root
Leaf
Variance (%)
n.s
**
(p=0.02)
**
(p=0.012)
***
(p=0.002)
16S SynCom (Root)
16S SynCom (Leaf)

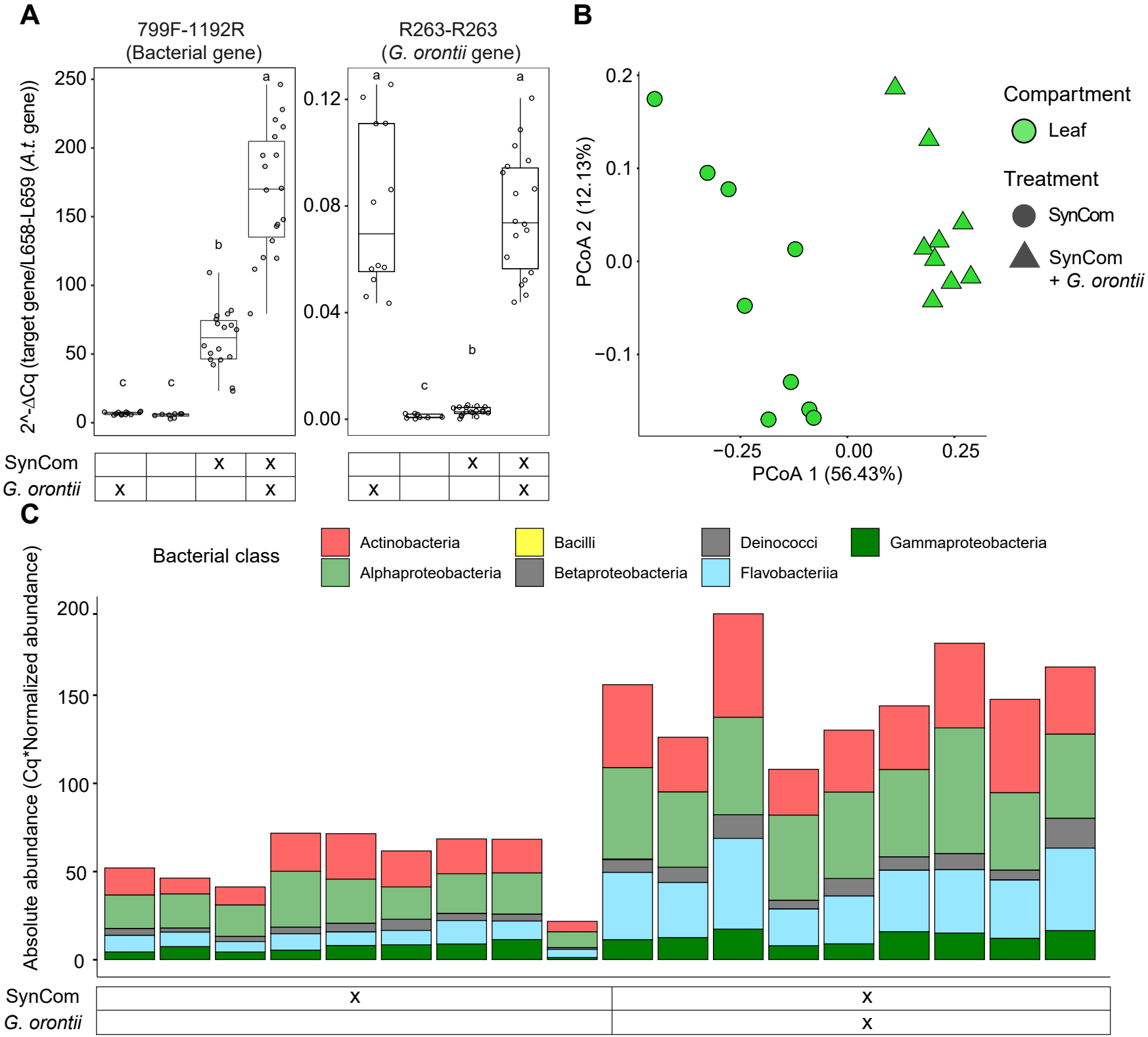
A
799F-1192R
(Bacterial gene)
R263-R263
(G. orontii gene)
2^-ΔCq (target gene/L658-L659 (A.t. gene))
SynCom
G. orontii
B
PCoA 2 (12.13%)
PCoA 1 (56.43%)
Compartment
Leaf
Treatment
SynCom
SynCom + G. orontii
C
Bacterial class
Actinobacteria
Alphaproteobacteria
Bacilli
Betaproteobacteria
Deinococci
Flavobacteriia
Gammaproteobacteria
Absolute abundance (Cq*Normalized abundance)
SynCom
G. orontii